

Motile dislocations knead odd crystals into whorls

Ephraim S. Bililign,¹ Florencio Balboa Usabiaga,^{2,3} Yehuda A. Ganan,¹ Alexis Poncet,⁴ Vishal Soni,¹ Sofia Magkiriadou,¹ Michael J. Shelley,^{3,5,*} Denis Bartolo,^{4,†} and William T. M. Irvine^{6,‡}

¹*James Franck Institute and Department of Physics, University of Chicago, Chicago, IL 60637, USA*

²*Basque Center for Applied Mathematics (BCAM), Alameda de Mazarredo 14, 48009 Bilbao, Spain*

³*Center for Computational Biology, Flatiron Institute, New York, NY 10010*

⁴*University of Lyon, ENS de Lyon, University of Claude Bernard, CNRS, Laboratoire de Physique, F-69342 Lyon, France*

⁵*Courant Institute, NYU, New York, NY 10012*

⁶*James Franck Institute, Enrico Fermi Institute and Department of Physics, University of Chicago, Chicago, IL 60637, USA*

The competition between thermal fluctuations and potential forces governs the stability of matter in equilibrium, in particular the proliferation and annihilation of topological defects. However, driving matter out of equilibrium allows for a new class of forces which are neither attractive nor repulsive, but rather transverse. The possibility of activating transverse forces raises the question of how they affect basic principles of material self-organization and control. Here, we show that transverse forces organize colloidal spinners into odd elastic crystals crisscrossed by motile dislocations. These motile topological defects organize into a poly-crystal made of grains with tunable length scale and rotation rate. The self-kneading dynamics drive super-diffusive mass transport, which can be controlled over orders of magnitude by varying the spinning rate. Simulations of both a minimal model and fully resolved hydrodynamics establish the generic nature of this crystal-whorl state. Using a continuum theory, we show that both odd and Hall stresses can destabilize odd-elastic crystals, giving rise to a generic state of crystalline active matter. Adding rotations to a material's constituents has far-reaching consequences for continuous control of structures and transport at all scales.

The celebrated interplay between configurational entropy and the energetics of topological defects in two-dimensional melting have provided a lens through which to understand the phases of condensed matter [16], such as superfluid films, colloids and liquid crystals [17–22]. While these systems span a wide range of particle interactions, scales, and intermediate phases, they are all unified in that the forces between constituents are primarily longitudinal, their dynamics are equilibrium, and their interactions are symmetric under both time-reversal and parity. What happens if the inter-particle interactions include transverse forces as well [1–9]? This deceptively minimal generalization can break these assumptions at a fundamental level.

In equilibrium, transverse forces cannot alter the phase behavior of condensed matter. However, there is no such

guarantee out of equilibrium and such transverse interactions generically occur in collections of naturally and artificially spinning objects. Examples include planetary disks [10], spinning cell aggregates and membrane inclusions [23, 24], active colloids and grains [4, 8, 9, 11–13, 25–27], atmospheric scale dynamics [28, 29], parity-breaking fluids [30–35] and simple models of turbulence [36]. How does this more general and ubiquitous form of matter generically self-organize, what are its stable phases, and how does it transition between them?

Figure 1a and Supplementary Movie 1 show a $\sim 200 \times 200 \mu\text{m}$ region within a centimetre-scale monolayer of magnetic colloids. Each particle is uniformly spun by an externally applied magnetic field, resulting in their self-organization into a dynamic and dense phase. The active rotation of the magnets gives rise to both longitudinal magnetic attraction and sustained chiral transverse hydrodynamic interactions, as illustrated in the inset of Figure 1a. Crucially, the forces are separation-dependent and can be tuned by varying the rotation frequency, providing an ideal platform for exploring how transverse interactions shape the dense phases of chiral matter.

Upon spinning our particles, we find that the system generically self-organizes into crystal ‘whorls’. A snapshot, colored by the phase of the crystalline bond-orientational order parameter, $\psi_6(\mathbf{x})$ (see Figure 1b and Supplementary Movie 2), reveals a polycrystalline arrangement of grains of triangular crystal order separated by topological defects organized into grain boundaries [37]. This picture is reminiscent of metallurgical crystalline phases with quenched disorder; however, unlike their crystalline static counterpart, the structure is continually evolving, grain boundaries move, collapse, and spontaneously emerge as crystalline domains rotate like vortical whorls (see Figure 1c and Supplementary Movie 3, 12). Segmenting the phase into crystalline domains enables us to study its statistical properties, revealing that after a short transient, the domains within this polycrystal settle to a constant characteristic size (SI Sec. 2.2). This scale can be tuned by altering the particle rotation rate alone, yielding either significantly larger or smaller crystalline whorls, as in Figure 3.

What powers this lively steady state? Careful inspec-

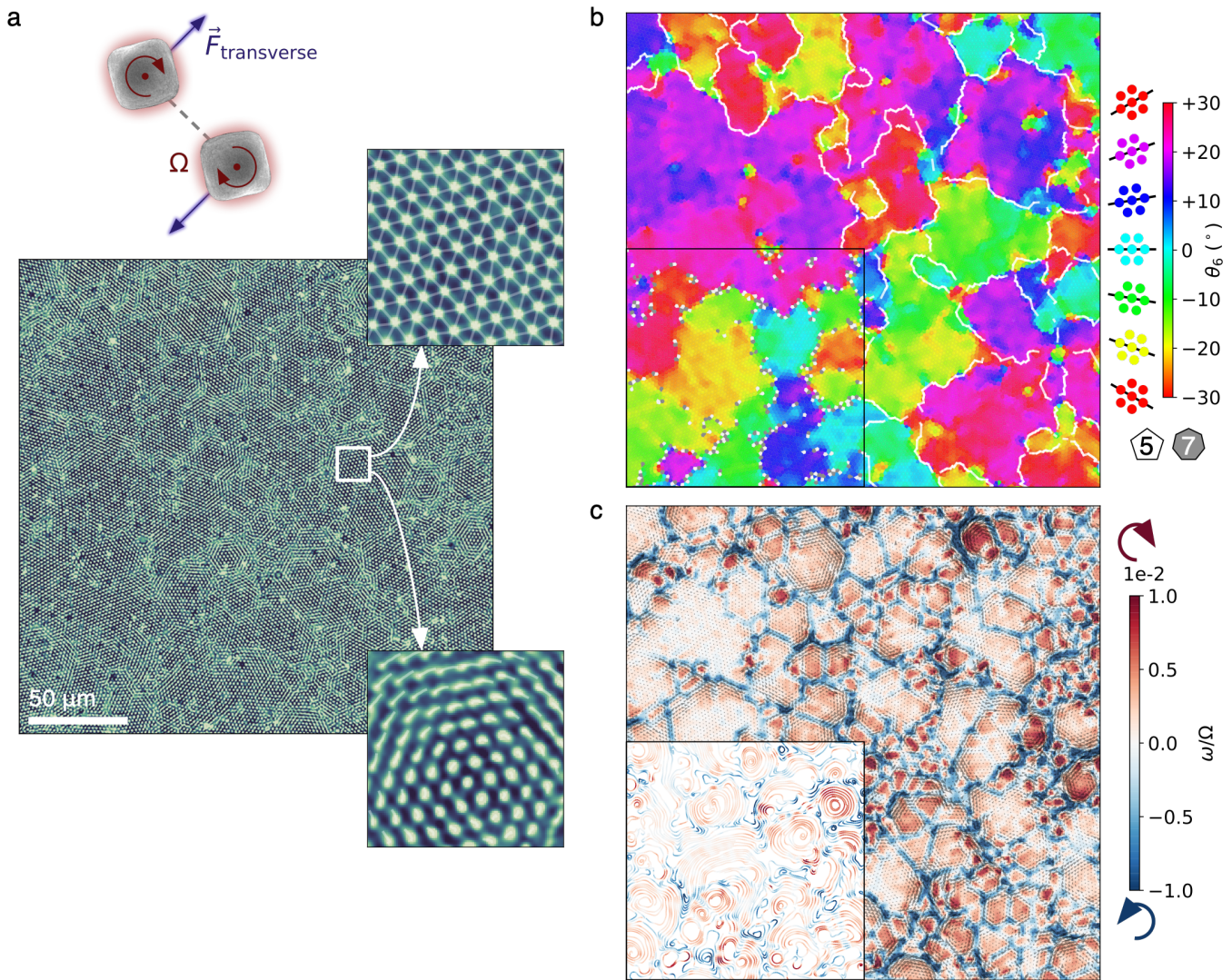


FIG. 1. **A crystal whorl state.** **a**, A dense and dynamic phase of colloids spinning at a frequency Ω and interacting through both longitudinal and transverse pairwise interactions is directly imaged with a microscope through crossed polarizers. The rotation-averaged position of each particle appears as a bright spot and reveals intermittent crystalline order (see Supplementary Movie 1). Magnifying a region reveals a highly-ordered crystalline structure (top), and time-averaging further reveals a rotating flow (bottom). **b**, To further illuminate the polycrystalline structure of this phase, we color particles by the angle of the local bond-orientational order parameter θ_6 . The polycrystal can be segmented into domains, and boundaries are drawn between them (see Supplementary Movie 2). The inset highlights the individual defects between grains, underlying grain boundaries. **c**, The polycrystal is dynamical and displays intermittent vortical flows as revealed when each region is colored by its vorticity ω (see Supplementary Movie 3). The inset presents the same vortical information through the streamlines of the particle flow (see Supplementary Movie 12).

tion reveals that the motion of topological defects in the crystalline structure is unlike the familiar motion of dislocations found in conventional passive materials. Conventional dislocations are either stationary or diffuse bidirectionally driven by thermal fluctuations; we observe instead that in our chiral medium they move ballistically as seen in Figure 2a and Supplementary Movie 4.

We can gain an intuitive understanding of what powers dislocation motility by inspecting the plastic deforma-

tions of the crystal brought about by dislocation glide. As shown in Figure 2b, dislocation glide reflects the displacement of one crystal plane over the other. As this deformation is equal parts rotation and shear, it is naturally actuated by the rotational drive.

To isolate this phenomenon, we introduce a minimal model of the overdamped dynamics of spinners interacting via transverse, frequency-dependent forces and potential longitudinal forces (SI Sec. 4.1). This minimal

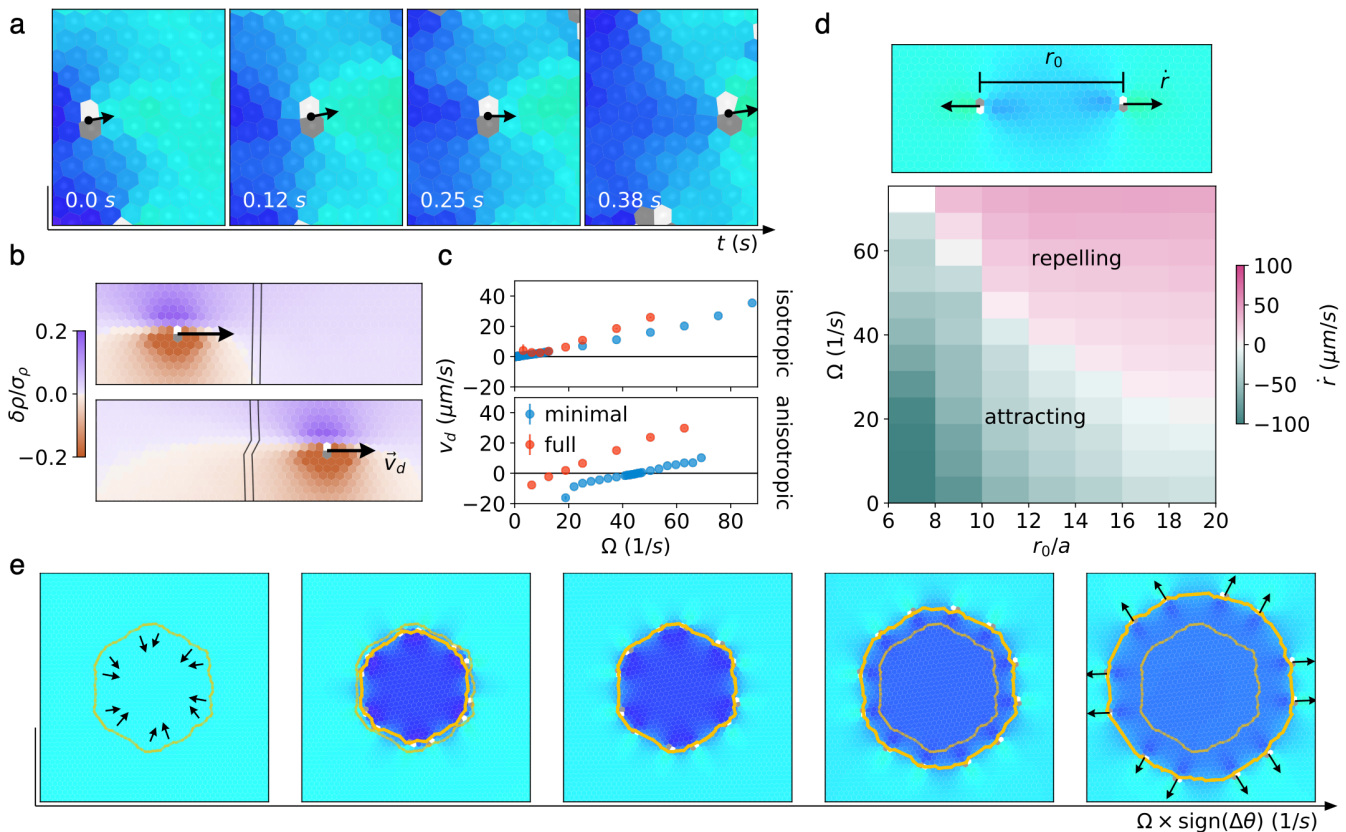


FIG. 2. **Motile dislocations.** Dislocations in the chiral crystalline phase behave like active particles. **a**, In the experiment, dislocations are observed to move ballistically in the direction of their Burgers vector. Same colormap as in Figure 1b. **b**, This behavior is reproduced in simulations of both the full hydrodynamic and minimal models by initializing a configuration corresponding to a single dislocation in an otherwise undefected crystal. In a crystal of particles interacting via transverse forces, we can intuit the dislocation’s direction of motion from the relative displacement of the crystal, which is colored by the relative density $\delta\rho = \rho - \bar{\rho}$ normalized by the standard deviation σ_ρ . **c**, The precise dislocation speed depends weakly on the details of the interactions. In both the minimal and full hydrodynamic models, the speed increases with frequency for isotropic dipole interactions (top). By contrast, dislocation motility is reversed at a frequency threshold for anisotropic dipole interactions (bottom). Error bars represent fit covariance (minimal) and standard error (full). **d**, By tuning the frequency and initial separation, two defects that would otherwise attract and annihilate can be made to repel, overwhelming even elastic forces with transverse ones. Same colormap as in Figure 1b. **e**, The collective dynamics of many defects arranged to form a grain boundary inherits this sensitivity to transverse forces. Such a grain boundary collapses when elastic forces dominate, and expands without bound when transverse forces dominate. Same colormap as in Figure 1b, orange line indicates position of grain boundary in both initial and present state for comparison.

approach is informed by full hydrodynamic simulations of particles that closely approximate our experimental system (SI Sec. 5.1). The transverse forces arise primarily from near-field hydrodynamic interactions, while the longitudinal interactions arise primarily from both steric repulsion and magnetic attraction (SI Sec. 5.5).

By initializing simulations with a single dislocation in an otherwise perfectly ordered triangular crystal (see Supplementary Movies 5-6), we are able to observe the motion of dislocations isolated from interactions with other defects in both minimal and full hydrodynamic simulations. As shown in Figure 2c, we observe that the glide speed is frequency dependent. When the longitudinal interactions between particles are isotropic, correspond-

ing to time-averaged magnetic interactions (SI Sec. 4.5, 5.3), the glide velocity is a monotonically increasing function, with a threshold (Figure 2c, SI Sec. 4.5.1). This is consistent with the notion of a unidirectional propulsion resisted by local Peierls barrier [39, 40]. In the case of anisotropic dipolar interactions, at low frequencies we observe a correction to defect propulsion brought about by a competition between magnetic and rotational interactions (Figure 2c).

The motility of individual dislocations provides a significant twist on the collective dynamics of defects normally driven by elastic interactions [41–46]. For example two defects that would normally attract and annihilate in response to elastic forces, can instead unbind when

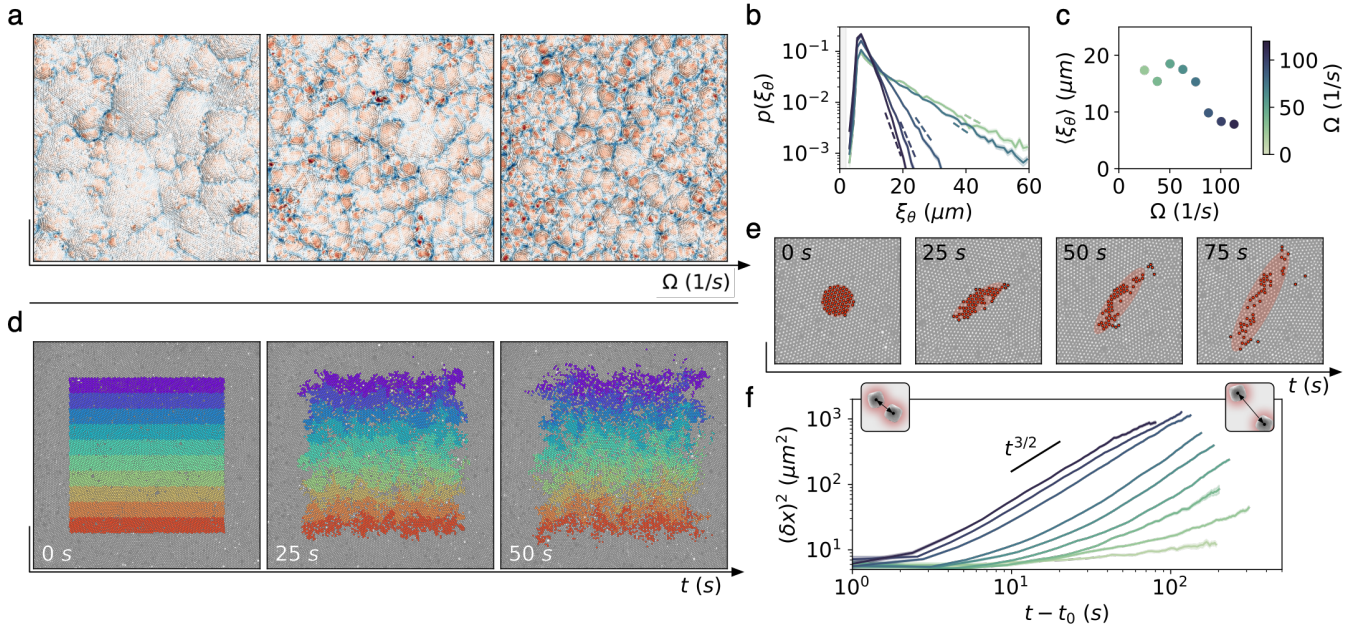


FIG. 3. **Transport in the crystalline whorl state.** **a**, The self-kneading of crystalline patches of material is tunable through the rotation frequency to yield a range of scales. Same colormap as in Figure 1c. **b**, These states are characterized by an exponential distribution of grain sizes, dashed straight lines represent the slope of the associated exponential fit. **c**, Accordingly, the average size of grains in the steady-state tends to decrease with frequency. Error bars, which are smaller than markers, represent standard error. **d**, The constant structural kneading of the chiral whorl state by topological defects introduces novel mixing properties which can be imaged by artificially dyeing stratified layers in a crystal that subsequently bleed into each other. **e**, By contrast to conventional diffusive processes, the smearing of the fluid over time is a strongly anisotropic process, wherein an example blob of fluid is pulled apart by the flow between two chiral whorls. **f**, The pairwise separation $(\delta x)^2$ plotted versus time t for particles initially in close proximity suggests that this abnormal spreading gives rise to superdiffusive behavior, which itself is a function of rotational frequency. Error bars represent standard error.

propelled by transverse forces as shown in Figure 2d.

The collective dynamics of several defects is similarly affected. Figure 2e shows snapshots from simulations in which we initialized a finite size grain in an otherwise perfect crystal and varied the rotation frequency (see Supplementary Movies 7-8). Altering the frequency affects transverse interactions most strongly and thus enables us to tune the balance between stabilizing elastic interactions and defect motility. As shown in Figure 2e, the grain size is set by the competition between motility and defect interactions. At low rotation frequencies the grains are stable, and their size becomes larger when the defect's propulsion direction is outwards. Similarly, they shrink and collapse for inwards defect motility. When the system is driven sufficiently strongly, the defect motility overpowers the elastic interactions resulting in unstable grain boundaries.

In the polycrystalline state we observe in our experiments, the instability of grain boundaries results in the exchange of dislocations between adjacent grains, as well as defect proliferation. These nonlinear dynamics drive the system to the dynamical crystal whorl state erasing any memory of the initial configuration.

The flow field $\mathbf{v}(\mathbf{x}_i)$ that emerges from the combina-

tion of motility and proliferation can be readily measured from individual particle trajectories and its corresponding vorticity $\omega(\mathbf{x}_i)$ is shown in Figure 1c. When time-averaged, this flow field corresponds to a quiet bulk (SI Sec. 2.3) and a lively edge [7]. However our time-resolved measurements reveal instantaneous dynamics shaped by unsteady vortical flows illustrated in Figure 1c. The dynamical and structural pictures of this chiral whorl state are aligned. As seen in Figure 1b-c, the grain boundaries support strongly localized flows having a vorticity opposite to the particle rotation. By contrast, the grains correspond to low positive vorticity, intermittently interrupted by isolated dislocations zipping through.

In this chaotic stationary state, the balance between even and odd forces remains the controlling parameter that determines the characteristic size of the chiral whorls, which can be viewed through the vorticity in Figure 3a and the distribution of crystalline grains in Figure 3b-c (SI Sec. 2.2-2.3, 4.4, 5.2). The sustained proliferation and annihilation of motile dislocations is reminiscent of active nematics where motile disclinations power spatiotemporal chaos [47]. Here dislocations give rise to self-kneading crystal whorls.

This self-kneading of the crystal phase results in en-

hanced mixing which can be qualitatively captured by artificially tagging the colloids and watching them spread; see Figure 3d and Supplementary Movie 11. As shown in Figure 3e, an artificially dyed blob spreads anisotropically before disintegrating into separate blobs, hinting at a mechanism reminiscent of Richardson diffusion in turbulence. We investigate this quantitatively by tracking the mean squared separation between pairs of particles in the chiral phase. Figure 3f shows that pair separation is super-diffusive above a separation that corresponds to the characteristic grain size due to a punctuated mix of conventional diffusion within crystalline whorls and Richardson-like diffusion between them. Note that tuning the frequency of rotation alters both the basic unit of time as well as the domain size (Figure 3d and e) enabling effective diffusion rates to be tuned over orders of magnitude.

Is the crystal whorl state generic? We repeated the experiments shown in Figure 1 while varying the applied magnetic field strength, adding a static vertical component of magnetic field, and varying the shape of the magnetic particles (SI Sec. 2.6). Additionally, we varied the microscopic interactions in our minimal model simulations (SI Sec. 4.8). Finally, in full hydrodynamic simulations, we simulated spheres and cubes that interact both magnetically and via isotropic attraction potentials (SI Sec. 5.2). In all cases we find that when transverse interactions dominate, the systems self-organizes into a crystal whorl state, supporting the notion that this state is generic. To gain further insight into the origins of this new state of matter, we adopt a continuum perspective and investigate destabilization mechanisms within this approach. As illustrated in Figure 4, the microscopic rotational drive induces transverse interactions between the constituent particles which in turn give rise to active stresses in the crystal phase. To gain an essential insight, we first consider the simplified case of a material in which neighboring particles interact via constant pairwise transverse forces. Figure 2, shows how such interactions naturally give rise to a uniform anti-symmetric odd stress [7, 48, 49], as well as all elastic moduli that can arise in an isotropic solid when energy conservation cannot be assumed [50]. As shown in Figure 4b-c, the moduli originate geometrically through the changes in perimeter of an infinitesimal material patch. A dilation (b) does not alter the total force on the edge, but increases the perimeter, thereby coupling dilation and rotational stress. Similarly, a shear deformation (c) alternately increases and decreases the length of the edges giving rise to a rotated shear stress (SI Sec. 6.2).

The addition of spatial dependence to the interaction forces (SI Sec. 6.3) makes estimating the moduli more challenging, however it does not alter the basic conclusion that a crystal of spinning particles is a quintessential odd elastic solid. Measuring the deformation field in a collection of nearly-circular, mono-crystalline droplets

(Figure 4e-f) provides corroborating evidence from experiments and simulations. The droplets rotate at a constant angular velocity that decreases with their radius R . Regardless of the droplet size, they consistently display a radial strain profile that varies from compressive in the center to dilational on the edge. Within an elastic description, this qualitative feature must originate from odd-elastic moduli. A continuum prediction of the strain field (SI Sec. 7.2) confirms this intuition and predicts the shape of the density profile, as illustrated in Figure 4d.

A natural question to ask is then whether odd elastic solids powered by odd stresses are linearly stable. We consider the continuum description of an elastic solid with a local displacement $\mathbf{u}(\mathbf{r}, t)$ and local velocity $\mathbf{v}(\mathbf{r}, t)$, that is allowed to experience all stresses consistent with broken parity and time-reversal (SI Sec. 6.1, 8.1) [7, 50]. In addition to elastic contributions, the symmetric stress, includes even and odd viscous contributions $\sigma_{ij} = -p\delta_{ij} + K_{ijkl}\partial_k u_\ell + \eta_{ijkl}\partial_k v_\ell$. The inner drive imposed by the spinners is encoded by the antisymmetric stress $\sigma_{ij}^{\text{spin}} = 2\eta_R\epsilon_{ij}\Omega$. Ignoring inertia, the dynamics is given by the balance between viscoelastic stresses and substrate drag defined by a constant friction coefficient Γ :

$$\Gamma\mathbf{v} = \nabla \cdot \boldsymbol{\sigma} + \nabla \cdot \boldsymbol{\sigma}^{\text{spin}}, \quad (1)$$

and the continuity equation $\partial_t \rho + \nabla \cdot (\rho\mathbf{v}) = 0$.

Linearizing about a homogeneous quiescent base state $\mathbf{u} = \mathbf{v} = 0$ and $\rho = \rho_0$ and making the ansatz $\mathbf{u}, \mathbf{v}, \rho \propto \exp(-i\omega t + i\mathbf{k} \cdot \mathbf{r})$, we readily obtain an expression for the dispersion $\nu \equiv \text{Re}(\omega)$ and damping $\alpha \equiv \text{Im}(\omega)$ of displacement and density waves (SI Sec. 8.2). We find a generic scenario yielding exponential amplification of density fluctuations. A number of different combinations of off-diagonal material parameters in $\boldsymbol{\eta}$ and \mathbf{K} result in different instabilities. However, they all reflect the same mechanistic picture, sketched in Figure 5a. A density fluctuation is converted to a localized rotation. The resulting net shear across the density fluctuation is in turn converted into an outward force amplifying the initial perturbation and so on to defect unbinding. Competition with the stabilizing influence of the conventional bulk and shear moduli of the elastic solid determine the consistent shape of the dispersion curves shown in Figure 5a and SI Sec. 8.2. Crucially, this generic mechanism relies on the coupling between stresses and strains having different spatial symmetries, which is only allowed when time reversal and parity symmetries are broken at the microscopic level [50, 51].

To test this simplified model, we measure the flows $\mathbf{v}(\mathbf{x})$ that occur in the bulk of a large crystallite driven at finite rotation frequency (see Supplementary Movie 10), and measure the Fourier spectrum of all scalar measures of deformation, including velocity and strain rate (SI Sec. 2.4). Figure 5b shows that following the onset of rotations the azimuthally averaged spectra evolve before

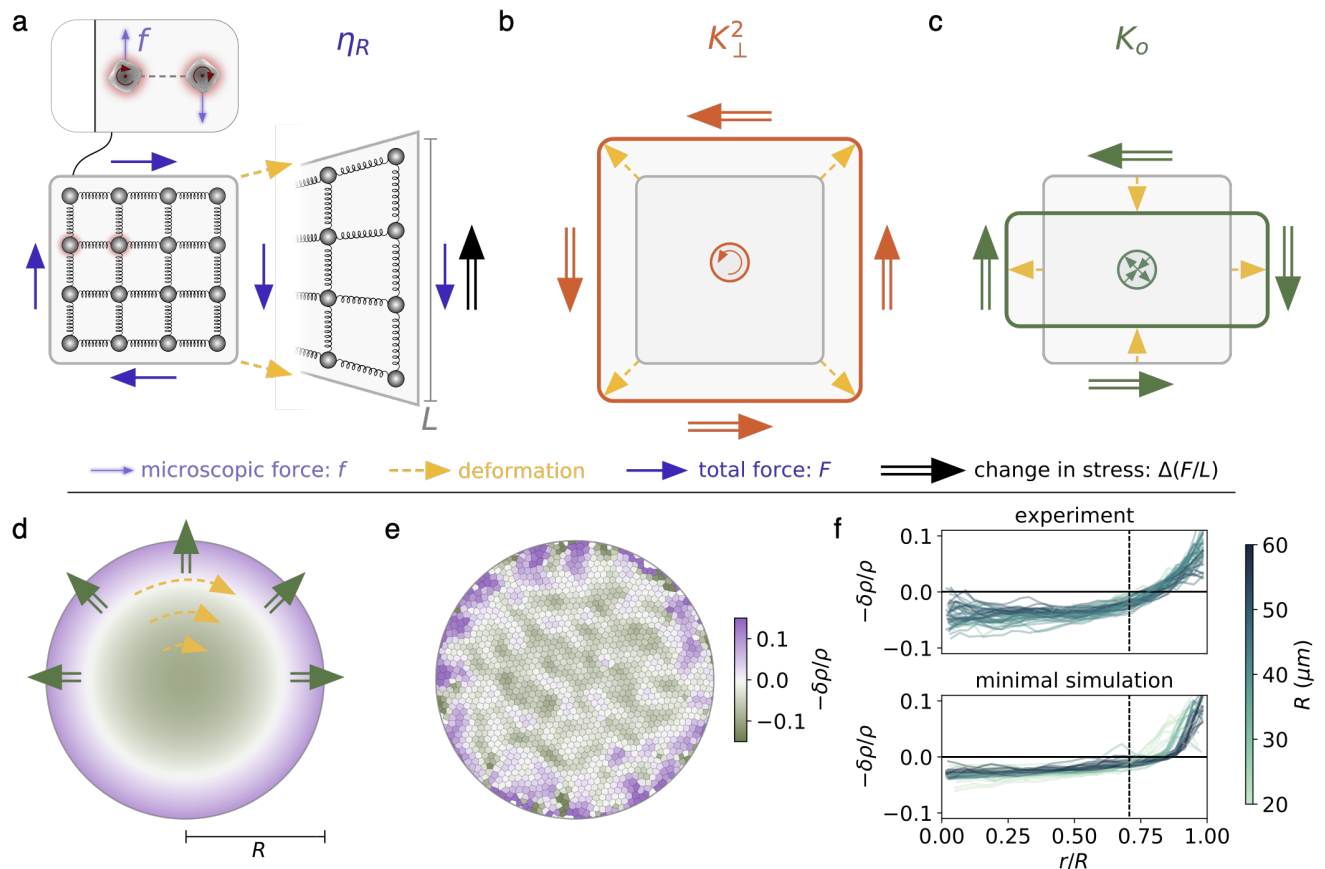


FIG. 4. **Odd response in the steady-state.** **a**, A patch of material built of particles that interact with their neighbors via constant, separation-independent transverse forces f parallel to the material's edge sustains a net odd stress $2\eta_R\Omega = nf/L$ on its edge, where n is the number of particles on an edge of length L (see SI Sec. 6.2 for a more general discussion). On each edge, the macroscopic total force $F = nf$ is unchanged upon dilating the edge, but as the length L of the boundary is increased, there is a net change in stress $\Delta(F/L)$ in a direction opposite to the odd stress. **b**, For a uniform dilation, the deformation leads to a net counter-rotational stress. This coupling between dilation and rotation is denoted by K_{\perp}^2 in the elasticity tensor. **c**, Likewise, for a shear deformation, the system acquires a net rotated shear stress, representative of the odd elasticity K_o . **d**, In a droplet of crystalline material, the odd stress induces a net rotation, balanced by friction with the substrate. The naturally occurring azimuthal distortion generates, via the odd elastic moduli, a characteristic radial density dependence (SI Sec. 7.2). **e**, We observe this signature of odd elastic response in experiments on droplets by measuring the dilational component of the strain through the relative density $\delta\rho/\rho$. **f**, In both the experiments and simulations, $\delta\rho/\rho$ transitions radially within a droplet from contracting to dilating in a manner independent of droplet radius R . In both cases, we obtain excellent qualitative agreement with the theoretical prediction for the transition radius, denoted by the dashed line (SI Sec. 7.2).

eventually settling into a steady state. By comparing the spectra at different times, we extract the mode growth curves shown in Figure 5 for (c) experiments and (f, g) simulations (SI Sec 2.4, 4.8, 5.4). They reveal the presence of an instability at finite wavelength for all modes with relatively constant growth above a characteristic scale. As shown in Figure 5c, a spatial map of the integrated growth rate reveals that this instability is consistent with the destabilization of our chiral crystal.

We note, however, that in finite crystalline domains, defects are readily produced at the boundary. Their subsequent propulsion into the bulk could curtail or otherwise affect the full development of the instability. Cru-

cially, we have not observed the spontaneous appearance of defects in the middle of a crystallite in our experiments. These combined observations suggest the existence of an additional mechanism for destabilization in which motile defects nucleate at the boundary and invade the crystal phase, actively fracturing the bulk into whorls.

Our minimal model simulations provide an ideal arena to investigate this possibility. By varying microscopic interaction parameters, we can tune the system from linearly stable to linearly unstable (SI Sec. 4.8.1). Remarkably, in both the stable and the unstable regime, we observe that initially perfectly crystalline droplets are

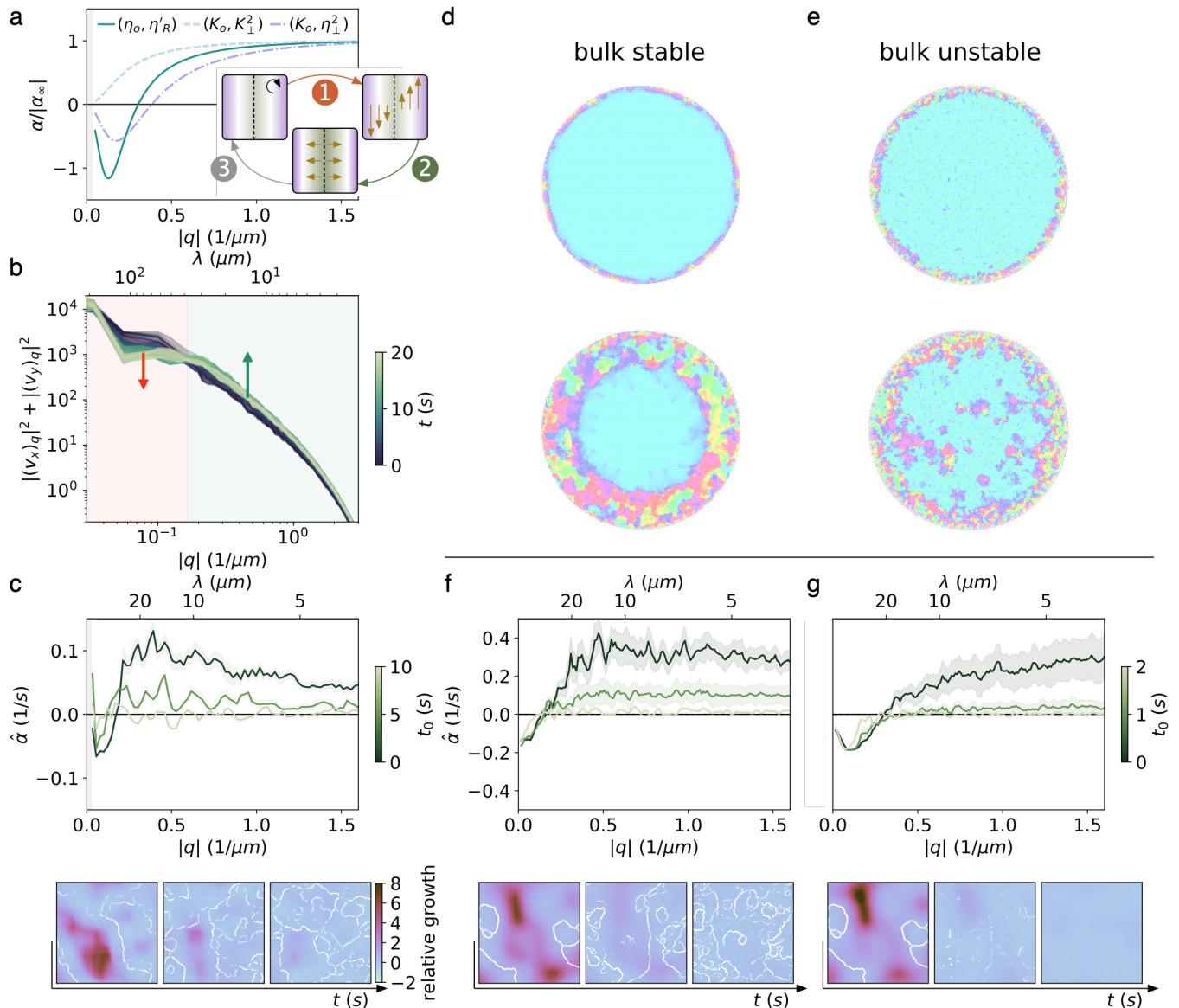


FIG. 5. Measuring an elasto-hydrodynamic instability. **a**, The chiral phase responds to a perturbation in spinner density by (1) coupling internal rotations to flow gradients that are (2) transformed into Hall stresses that (3) destabilize the crystal further (SI Sec. 8.1). A linear stability analysis of this model yields the predicted spectral growth curves arising from the interplay between odd transport coefficients (η_o, K_o) and Magnus-like couplings ($\eta'_R, K'_\perp, \eta'_\perp$). **b**, As the chiral phase approaches the steady-state of Figure 1, we can measure the spectrum of its flow to see decay at large scales and growth at small scales. **c**, The total amount of growth measured at these smaller scales can be mapped over time and compared to the grain boundaries to reveal enhanced growth within initially crystalline patches and vanishing growth at later times (SI Sec. 2.4). The estimated spectrum of growth $\hat{\alpha}(q)$ reveals stabilization at scales $\lambda \gg \langle \xi_\theta \rangle$ and constant destabilization at scales $\lambda \ll \langle \xi_\theta \rangle$. **d**, In simulations, we tune the inter-particle interaction range to prepare a theoretically stable crystal, for which the crystal is destabilized through dislocation production to reach the whorl state. **e**, Likewise, simulations that are theoretically unstable can go unstable in response to bulk density fluctuations. Same colormap as in Figure 1b. **f**, The estimated spectrum and spatial map of growth for a theoretically stable simulation resembles the experiment when a polycrystal is destabilized. **g**, The same signatures are observed in a linearly unstable simulation. **f-g** use the same colormap as **c**.

destabilized by the production of defects at the edges of the droplets, which subsequently invade the bulk in a visible front (Figure 5d-e). The only difference is that deep in the unstable regime (e), we also observe defect nucleation in the bulk of the droplet before the front arrives.

Notably, in both cases a crystal whorl emerges as the steady state (SI Sec. 4.8.2). This mechanism of destabilization has a different origin from the linear instability described above; within our continuum approach the presence of a constant background odd stress plays no

role in the crystal's stability, rather its primary effect is to drive defect propulsion (SI Sec. 7.3, 8.2.1).

Remarkably, measurements of the spectral growth in both regimes, performed for simulations initialized in a polycrystalline phase, display general shapes and spatial maps that are similar to those observed in the experiment (Figure 5f-g). The similar shape of the resulting curves demonstrates the challenge of disentangling the precise origin of the growth in terms of linear response coefficients.

Breaking parity by spinning a material's constituents gives rise to transverse forces that fundamentally alter the organization of matter. Spinner crystals generically melt into a dynamical state driven by motile dislocations. The resulting, tunable crystal-whorl state opens new avenues for control of structure and transport from synthetic materials to biological colonies.

Acknowledgments. We would like to acknowledge discussions with P. Wiegmann, A. Abanov, D. Nelson, C. Scheibner, M. Han, M. Fruchart, S. Gokhale, N. Fakhri and J. Dunkel. We thank V. Vitelli for an insightful discussion on the importance of odd stress on defect motility. We thank Wen Yan for useful conversations.

This work was primarily supported by the University of Chicago Materials Research Science and Engineering Center, which is funded by National Science Foundation under award number DMR-2011854. Additional support was provided by NSF DMR-1905974, NSF EFRI NewLAW 1741685 and the Packard Foundation. M.J.S. acknowledges the support from NSF grants DMR-1420073 (NYU-MRSEC) and DMR-2004469. D. B. acknowledges the support from ARN grant WTF and IDEX-Lyon Tore. E.S.B. was supported by the National Science Foundation Graduate Research Fellowship under Grant No. 1746045. D.B. and W.T.M.I. gratefully acknowledge the Chicago-France FACCTS programme. F.B.U. acknowledges support from "la Caixa" Foundation (ID 100010434), fellowship LCF/BQ/PI20/11760014, and from the European Union's Horizon 2020 research and innovation programme under the Marie Skłodowska-Curie grant agreement No 847648. The University of Chicago's Research Computing Center and the University of Chicago's GPU-based high-performance computing system (NSF DMR-1828629) are gratefully acknowledged for access to computational resources and the Chicago MRSEC (US NSF grant DMR-2011854) is also gratefully acknowledged for access to its shared experimental facilities.

Note to be added in proof. In the concluding stages of our work we became aware of a complementary, independent effort by the groups of N. Fakhri and J. Dunkel who studied parity breaking crystal dynamics in a biophysical system (unpublished).

* shelley@cims.nyu.edu

† denis.bartolo@ens-lyon.fr

‡ wtmirvine@uchicago.edu

- [1] Cafiero, R., Luding, S. & Herrmann, H. J. Rotationally driven gas of inelastic rough spheres. *EPL (Europhysics Letters)* **60**, 854 (2002).
- [2] Grzybowski, B. A., Stone, H. A. & Whitesides, G. M. Dynamic self-assembly of magnetized, millimetre-sized objects rotating at a liquid-air interface. *Nature* **405**, 1033–1036 (2000).
- [3] Yan, J., Bae, S. C. & Granick, S. Rotating crystals of magnetic Janus colloids. *Soft Matter* **11**, 147–153 (2014).
- [4] Nguyen, N. H., Klotsa, D., Engel, M. & Glotzer, S. C. Emergent Collective Phenomena in a Mixture of Hard Shapes through Active Rotation. *Physical Review Letters* **112** (2014).
- [5] Yeo, K., Lushi, E. & Vlahovska, P. M. Collective Dynamics in a Binary Mixture of Hydrodynamically Coupled Microrotors. *Physical Review Letters* **114** (2015).
- [6] Kokot, G., Piet, D., Whitesides, G. M., Aranson, I. S. & Snezhko, A. Emergence of reconfigurable wires and spinners via dynamic self-assembly. *Scientific Reports* **5** (2015).
- [7] Soni, V. *et al.* The odd free surface flows of a colloidal chiral fluid. *Nature Physics* **15**, 1188–1194 (2019).
- [8] Shen, Z. & Lintuvuori, J. S. Two-phase crystallization in a carpet of inertial spinners. *Phys. Rev. Lett.* **125**, 228002 (2020).
- [9] Liu, P. *et al.* Oscillating collective motion of active rotors in confinement. *Proceedings of the National Academy of Sciences* **117**, 11901–11907 (2020).
- [10] Armitage, P. J. Turbulence and angular momentum transport in a global accretion disk simulation. *The Astrophysical Journal Letters* **501**, L189 (1998).
- [11] Scholz, C., Engel, M. & Pöschel, T. Rotating robots move collectively and self-organize. *Nature Communications* **9**, 931 (2018).
- [12] Lim, M. X., Souslov, A., Vitelli, V. & Jaeger, H. M. Cluster formation by acoustic forces and active fluctuations in levitated granular matter. *Nature Physics* **15**, 460–464 (2019).
- [13] Aubret, A., Youssef, M., Sacanna, S. & Palacci, J. Targeted assembly and synchronization of self-spinning microgears. *Nature Physics* **14**, 1114–1118 (2018).
- [14] Jiang, W. *et al.* Direct observation of the skyrmion hall effect. *Nature Physics* **13**, 162–169 (2017).
- [15] Jülicher, F., Ajdari, A. & Prost, J. Modeling molecular motors. *Reviews of Modern Physics* **69**, 1269 (1997).
- [16] Chaikin, P. M., Lubensky, T. C. & Witten, T. A. *Principles of condensed matter physics*, vol. 10 (Cambridge university press Cambridge, 1995).
- [17] Strandburg, K. J. Two-dimensional melting. *Rev. Mod. Phys.* **60**, 161–207 (1988).
- [18] Bishop, D. J. & Reppy, J. D. Study of the superfluid transition in two-dimensional ^4He films. *Phys. Rev. Lett.* **40**, 1727–1730 (1978).
- [19] Zahn, K., Lenke, R. & Maret, G. Two-stage melting of paramagnetic colloidal crystals in two dimensions. *Phys. Rev. Lett.* **82**, 2721–2724 (1999).
- [20] Alsayed, A. M., Islam, M. F., Zhang, J., Collings, P. J. & Yodh, A. G. Premelting at defects within bulk colloidal

- crystals. *Science* **309**, 1207–1210 (2005).
- [21] Meng, G., Paulose, J., Nelson, D. R. & Manoharan, V. N. Elastic instability of a crystal growing on a curved surface. *Science* **343**, 634–637 (2014).
- [22] Thorneywork, A. L., Abbott, J. L., Aarts, D. G. A. L. & Dullens, R. P. A. Two-dimensional melting of colloidal hard spheres. *Phys. Rev. Lett.* **118**, 158001 (2017).
- [23] Petroff, A. P., Wu, X.-L. & Libchaber, A. Fast-moving bacteria self-organize into active two-dimensional crystals of rotating cells. *Physical review letters* **114**, 158102 (2015).
- [24] Oppenheimer, N., Stein, D. B. & Shelley, M. J. Rotating membrane inclusions crystallize through hydrodynamic and steric interactions. *Physical review letters* **123**, 148101 (2019).
- [25] van Zuiden, B. C., Paulose, J., Irvine, W. T. M., Bartolo, D. & Vitelli, V. Spatiotemporal order and emergent edge currents in active spinner materials. *Proceedings of the National Academy of Sciences* **113**, 12919–12924 (2016).
- [26] Snezhko, A. Complex collective dynamics of active torque-driven colloids at interfaces. *Current Opinion in Colloid & Interface Science* **21**, 65–75 (2016).
- [27] Kokot, G. *et al.* Active turbulence in a gas of self-assembled spinners. *Proceedings of the National Academy of Sciences* **114**, 12870–12875 (2017).
- [28] Bouchet, F. & Venaille, A. Statistical mechanics of two-dimensional and geophysical flows. *Physics reports* **515**, 227–295 (2012).
- [29] Baroud, C. N., Plapp, B. B., She, Z.-S. & Swinney, H. L. Anomalous self-similarity in a turbulent rapidly rotating fluid. *Physical Review Letters* **88**, 114501 (2002).
- [30] Korving, J., Hulsman, H., Knaap, H. & Beenakker, J. Transverse momentum transport in viscous flow of diatomic gases in a magnetic field. *Physics Letters* **21**, 5–7 (1966).
- [31] Hoyos, C., Moroz, S. & Son, D. T. Effective theory of chiral two-dimensional superfluids. *Physical Review B* **89**, 174507 (2014).
- [32] Wiegmann, P. & Abanov, A. G. Anomalous Hydrodynamics of Two-Dimensional Vortex Fluids. *Physical Review Letters* **113**, 034501 (2014).
- [33] Souslov, A., Dasbiswas, K., Fruchart, M., Vaikuntanathan, S. & Vitelli, V. Topological waves in fluids with odd viscosity. *Physical review letters* **122**, 128001 (2019).
- [34] Banerjee, D., Souslov, A., Abanov, A. G. & Vitelli, V. Odd viscosity in chiral active fluids. *Nature Communications* **8**, 1573 (2017).
- [35] Han, M. *et al.* Statistical mechanics of a chiral active fluid. *arXiv preprint arXiv:2002.07679* (2020).
- [36] Eyink, G. L. & Sreenivasan, K. R. Onsager and the theory of hydrodynamic turbulence. *Reviews of modern physics* **78**, 87 (2006).
- [37] Lavergne, F. A., Aarts, D. G. & Dullens, R. P. Anomalous grain growth in a polycrystalline monolayer of colloidal hard spheres. *Physical Review X* **7**, 041064 (2017).
- [38] Anderson, J. A., Glaser, J. & Glotzer, S. C. Hoomd-blue: A python package for high-performance molecular dynamics and hard particle monte carlo simulations. *Computational Materials Science* **173**, 109363 (2020).
- [39] Peierls, R. Reports on progress of physics. *The Physical Society, (London) Vol. VI* **78** (1939).
- [40] Nabarro, F. Dislocations in a simple cubic lattice. *Proceedings of the Physical Society* **59**, 256 (1947).
- [41] Schall, P., Cohen, I., Weitz, D. A. & Spaepen, F. Visualization of dislocation dynamics in colloidal crystals. *Science* **305**, 1944–1948 (2004).
- [42] Weinberger, C. R. & Cai, W. Surface-controlled dislocation multiplication in metal micropillars. *Proceedings of the National Academy of Sciences* **105**, 14304–14307 (2008).
- [43] Irvine, W. T. M., Hollingsworth, A. D., Grier, D. G. & Chaikin, P. M. Dislocation reactions, grain boundaries, and irreversibility in two-dimensional lattices using topological tweezers. *Proceedings of the National Academy of Sciences* **110**, 15544–15548 (2013).
- [44] Amir, A. & Nelson, D. R. Dislocation-mediated growth of bacterial cell walls. *Proceedings of the National Academy of Sciences* **109**, 9833–9838 (2012).
- [45] Deutschländer, S., Dillmann, P., Maret, G. & Keim, P. Kibble–zurek mechanism in colloidal monolayers. *Proceedings of the National Academy of Sciences* **112**, 6925–6930 (2015).
- [46] Braverman, L., Scheibner, C. & Vitelli, V. Topological defects in non-reciprocal active solids with odd elasticity. *arXiv preprint arXiv:2011.11543* (2020).
- [47] Sanchez, T., Chen, D. T., DeCamp, S. J., Heymann, M. & Dogic, Z. Spontaneous motion in hierarchically assembled active matter. *Nature* **491**, 431–434 (2012).
- [48] Dahler, J. S. & Scriven, L. E. Theory of Structured Continua. I. General Consideration of Angular Momentum and Polarization. *Proceedings of the Royal Society of London A: Mathematical, Physical and Engineering Sciences* **275**, 504–527 (1963).
- [49] Tsai, J.-C., Ye, F., Rodriguez, J., Gollub, J. P. & Lubensky, T. C. A Chiral Granular Gas. *Physical Review Letters* **94**, 214301 (2005).
- [50] Scheibner, C. *et al.* Odd elasticity. *Nature Physics* **16**, 475–480 (2020).
- [51] Epstein, J. M. & Mandadapu, K. K. Time-reversal symmetry breaking in two-dimensional nonequilibrium viscous fluids. *Phys. Rev. E* **101**, 052614 (2020).